Thiol reductive stress activates the hypoxia response pathway

Ravi[1], Ajay Kumar[2], Shalmoli Bhattacharyya[2], and Jogender Singh[1,3,*]

[1]Department of Biological Sciences, Indian Institute of Science Education and Research, Mohali, Punjab, India

[2]Department of Biophysics, Postgraduate Institute of Medical Education and Research, Chandigarh, India

[3]Lead contact

[*]Corresponding author: jogender@iisermohali.ac.in

Summary

Thiol antioxidants disrupt the oxidative protein folding environment in the endoplasmic reticulum (ER), resulting in protein misfolding and ER stress. We recently showed that thiol antioxidants modulate the methionine-homocysteine cycle by upregulating an S-adenosylmethionine-dependent methyltransferase, *rips-1*, in *Caenorhabditis elegans*. However, the changes in cellular physiology induced by thiol-mediated reductive stress that modulate the methionine-homocysteine cycle remain uncharacterized. Here, using forward genetic screens in *C. elegans*, we discover that thiol reductive stress enhances *rips-1* expression via the hypoxia response pathway. We demonstrate that thiol reductive stress activates the hypoxia response pathway and protects against hypoxic stress. Conversely, the hypoxia response pathway protects against thiol reductive stress. The activation of the hypoxia response pathway by thiol reductive stress is conserved in human cells. Finally, we show that enhanced cellular oxygen consumption by thiol reductive stress creates hypoxia. These studies reveal an intriguing interaction between thiol-mediated reductive stress and the hypoxia response pathway.

Keywords: Reductive stress, hypoxia, endoplasmic reticulum, *hif-1*, disulfide

Introduction

Maintenance of cellular homeostasis requires a balanced redox environment in the cell. Redox reactions result in the production of reactive oxygen species (ROS). High levels of ROS are associated with several pathological conditions (Sies and Jones, 2020). However, physiological ROS plays essential roles in cellular survival, differentiation, proliferation, repair, and aging (Sies and Jones, 2020; Trachootham et al., 2008). An increased amount of antioxidants results in the depletion of ROS, leading to reductive stress that is linked with several pathological conditions (Pérez-Torres et al., 2017; Rajasekaran, 2020). Dietary supplementation of high amounts of antioxidants correlates with accelerated cancer progression and a higher incidence of cancer-related mortality (Sayin et al., 2014; Villanueva and Kross, 2012). A high amount of dietary antioxidants accelerates aging in the nematode *Caenorhabditis elegans* (Gusarov et al., 2021). Despite the association of high amounts of

antioxidants with pathological conditions, the full spectrum of physiological effects of reductive stress remains to be elucidated.

Thiols, which contain a sulfhydryl group, are a major defense mechanism in the cell against oxidative stress and undergo oxidation to form disulfides under oxidative conditions (Ulrich and Jakob, 2019). Alterations in thiol-disulfide homeostasis play a role in several pathological conditions, including cardiovascular disease (Kundi et al., 2015), chronic renal disease (Rodrigues et al., 2013), and diabetes mellitus (Ates et al., 2016). However, the physiological effects of thiol reductive stress remain obscurely characterized. Because disulfide bonds are formed in the oxidative environment of the endoplasmic reticulum (ER), ER is expected to be the primary target of reductive stress (Cuozzo and Kaiser, 1999; Merksamer et al., 2008). Indeed, thiols such as dithiothreitol (DTT) disrupt disulfide bonds in the ER, leading to protein misfolding (Braakman et al., 1992). The ensuing protein misfolding results in ER stress; therefore, thiol reducing agents are used as ER-specific stressors (Oslowski and Urano, 2011). In addition to ER stress, thiol antioxidants can also result in oxidative stress by activating futile oxidative cycles in the ER (Maity et al., 2016). Recent studies in *C. elegans* showed that, besides causing ER stress, thiol antioxidants modulate the methionine-homocysteine cycle (Gokul and Singh, 2022; Winter et al., 2022). The modulation of the methionine-homocysteine cycle is a consequence of the upregulation of an S-adenosylmethionine (SAM)-dependent methyltransferase, *rips-1*, by thiol antioxidants. Thus, reductive stress caused by thiols could affect cellular physiology beyond the ER. However, such physiological effects of thiol antioxidants remain to be fully characterized.

In this study, using *C. elegans* and human cell lines, we characterized the physiological effects of thiol reductive stress. Because thiols antioxidants result in the increased expression of *rips-1* (Gokul and Singh, 2022; Winter et al., 2022), we reasoned that understanding the regulation of *rips-1* expression might provide insights into the physiological effects of thiol reductive stress. To this end, we carried out forward genetic screens to understand the regulation of *rips-1* expression. The expression levels of *rips-1* correlated with the activity of the hypoxia response pathway. We observed that exposure to DTT resulted in the activation of a functional hypoxia response pathway that protected against hypoxic stress. Further, the hypoxia response pathway protected against thiol reductive stress. The activation of the hypoxia response pathway by DTT exposure is conserved in human cell lines. We showed that thiol reductive stress creates hypoxia through

enhanced consumption of cellular oxygen. These studies reveal an intriguing relationship between thiol reductive stress and the hypoxia response pathway.

Results

The hypoxia response pathway modulates *rips-1* expression levels

The thiol antioxidants, DTT and β-mercaptoethanol, cause toxicity in *C. elegans* by upregulating a SAM-dependent methyltransferase, *rips-1*, that results in the modulation of the methionine-homocysteine cycle (Gokul and Singh, 2022; Winter et al., 2022). Mitochondrial dysfunction and the hypoxia-inducible factor might alter *rips-1* expression (Winter et al., 2022); however, the full spectrum of physiological changes induced by thiol reductive stress that results in the upregulation of *rips-1*, remains to be discovered. To characterize the physiological changes that trigger the upregulation of *rips-1*, we designed a forward genetic screen to isolate mutants that had constitutive activation of *rips-1*, utilizing a *rips-1p::GFP* reporter strain (Figure S1). We obtained three independent mutants that had enhanced green fluorescent protein (GFP) expression compared to the parental strain JSJ13 (*rips-1p::GFP*) (Figures 1A and 1B).

To identify the causative mutations, we performed whole-genome sequencing of the mutants after backcrossing them six times with the parental strain. The sequenced genomes of mutants were aligned with the reference genome of *C. elegans* to identify variants. Evaluation of the protein-coding genes having mutations in the isolated mutants revealed that all of the mutants had mutations in different negative regulators of the hypoxia response pathway (Figure 1C). The JSJ14 mutant animals had two missense mutations in the gene *rhy-1*, the JSJ15 mutant animals had a splice site acceptor mutation in the gene *egl-9*, and the JSJ16 mutant animals had a premature nonsense mutation in the gene *vhl-1* (Figure 1C). Because *egl-9(jsn15)* and *vhl-1(jsn16)* are likely loss-of-function alleles, these data suggested that inhibition of the negative regulators of the hypoxia response pathway may result in the enhanced expression of *rips-1*. Indeed, the knockdown of *egl-9*, *rhy-1*, and *vhl-1* by RNA interference (RNAi) resulted in the upregulation of *rips-1p::GFP* (Figures 1D and 1E).

The genes *egl-9*, *rhy-1*, and *vhl-1* are involved in the degradation of the transcription factor hypoxia-inducible factor 1 (HIF-1) (Epstein et al., 2001; Shen et al., 2006). Inhibition of these genes results in the accumulation of HIF-1 and activates the expression of hypoxia

response genes (Shen et al., 2006). We asked whether the upregulation of *rips-1* also required HIF-1. To this end, we exposed the *hif-1(ia4);rips-1p::GFP* animals to DTT and monitored changes in GFP levels. The *hif-1(ia4)* allele is a predicted null allele with deletion of exons 2–4 and lacks the induction of hypoxia response genes (Shen et al., 2005). While DTT exposure resulted in high GFP levels in *rips-1p::GFP* animals, GFP levels did not increase in *hif-1(ia4);rips-1p::GFP* animals (Figures 1F-1H). Taken together, these data indicated that the hypoxia response pathway regulates the expression of *rips-1*.

CYSL-1 is required for DTT-mediated *rips-1* upregulation

To better understand the interplay between *rips-1* expression and the hypoxia response pathway, we carried out another forward genetic screen to isolate mutants that failed to upregulate *rips-1* upon exposure to DTT—a phenotype similar to *hif-1* loss-of-function mutants (Figure S2A). We isolated two mutants that failed to upregulate *rips-1* upon exposure to DTT (Figures 2A-2D). To identify the causative mutations, the variants in the mutant animals were identified by whole-genome sequencing. Evaluation of the protein-coding genes having mutations in the linked regions revealed that both mutants had a missense mutation in the gene *cysl-1* (Figure 2E). Previous studies have identified *cysl-1* as a positive regulator of the hypoxia response pathway that inhibits *egl-9* activities (Ma et al., 2012; Wang et al., 2022).

Because *cysl-1* may act upstream or downstream of *hif-1* depending on the context (Budde and Roth, 2011; Ma et al., 2012), we carried out an epistasis analysis of *cysl-1* with the other components of the hypoxia response pathway in the context of *rips-1* expression. To this end, we knocked down *egl-9*, *rhy-1*, and *vhl-1* genes in *cysl-1(jsn17);rips-1p::GFP* and *cysl-1(jsn18);rips-1p::GFP* animals and monitored the changes in GFP expression. Knockdown of *egl-9* and *vhl-1* resulted in the upregulation of *rips-1* in both the alleles of *cysl-1*, while no upregulation of *rips-1* was observed upon knockdown of *rhy-1* (Figures 2F and 2G; Figures S2B and S2C). In line with previous observations (Ma et al., 2012), these results indicated that *cysl-1* acts downstream of *rhy-1* and upstream of *egl-9* and *vhl-1*.

Thiol reductive stress activates the hypoxia response pathway

The involvement of the hypoxia response pathway in DTT-mediated upregulation of *rips-1* suggested that thiol reductive stress may activate the hypoxia response pathway. To test this possibility, we exposed *nhr-57p::GFP* animals to DTT. The gene *nhr-57* is known to be upregulated by HIF-1 under hypoxic conditions (Shen et al., 2005). DTT exposure resulted in the upregulation of GFP in *nhr-57p::GFP* animals (Figures 3A and 3B). The endogenous mRNA levels of *nhr-57* were also induced in animals exposed to DTT (Figure 3C). We analyzed the mRNA levels of several other genes that are induced by hypoxia, including *cysl-2*, *rhy-1*, *fmo-2*, *sqrd-1*, *gst-19*, and *oac-54* (Shen et al., 2005). All of these genes had significantly increased levels in DTT-exposed animals compared with the control animals (Figure 3C). The DTT-mediated induction of most of the hypoxia-response genes was dependent on *hif-1* (Figure 3D). The only exceptions were *nhr-57* and *fmo-2*. The upregulation of *nhr-57* was partially dependent on *hif-1*, while the upregulation of *fmo-2* was independent of *hif-1* (Figures 3C and 3D). The expression of *fmo-2* under hypoxic conditions is known to be regulated by the transcription factor NHR-49 (Doering et al., 2022). Taken together, these studies showed that DTT exposure results in the activation of HIF-1-mediated hypoxia response.

Next, we asked whether DTT activated a functional hypoxia response. Enhanced activity of the hypoxia response pathway has been shown to impart resistance to hydrogen cyanide-mediated fast paralytic killing of *C. elegans* by *Pseudomonas aeruginosa* PAO1 (Gallagher and Manoil, 2001). We observed that pre-treatment with DTT enhanced the resistance of wild-type N2 animals to fast paralytic killing by *P. aeruginosa* PAO1 (Figure 3E). The hypoxia response pathway mutants exhibited enhanced susceptibility to *P. aeruginosa* PAO1 (Figures 3F and 3G), confirming the requirement of the hypoxia response pathway to protect against paralytic killing by *P. aeruginosa* PAO1. Importantly, pre-treatment with DTT did not enhance the survival of the hypoxia response pathway mutants (Figures 3F and 3G). These results indicated that DTT activates a functional hypoxia response that protects *C. elegans* against hypoxic stress induced by *P. aeruginosa* PAO1-produced hydrogen cyanide.

Hypoxia response pathway protects against thiol reductive stress

Next, we asked whether activation of the hypoxia response pathway conferred any protection against thiol reductive stress. Thiol antioxidants-mediated upregulation of *rips-1* modulates

the methionine-homocysteine cycle and results in developmental toxicity (Gokul and Singh, 2022; Winter et al., 2022). Therefore, it appeared that the activation of the hypoxia response pathway by thiol antioxidants, which results in the upregulation of *rips-1*, might be harmful to the host. To understand the role of the hypoxia response pathway in toxicity by thiol reductive stress, we studied the response of *hif-1(ia4)*, *cysl-1(jsn17)*, and *cysl-1(jsn18)* animals to varying concentrations of DTT. Compared to wild-type N2 animals, *hif-1* and *cysl-1* loss-of-function mutants had improved development on 5 and 7.5 mM DTT (Figures 4A-4D; Figures S3A-S3C). However, at 10 mM DTT, the hypoxia response pathway mutants failed to develop, similar to the wild-type animals.

Because vitamin B12 restores the DTT-modulated methionine-homocysteine cycle, vitamin B12 alleviates DTT toxicity in wild-type animals (Gokul and Singh, 2022; Winter et al., 2022). Despite lacking induction of *rips-1*, the hypoxia response pathway mutants failed to develop on 10 mM DTT (Figures 4A-4D). Therefore, we asked whether supplementation of vitamin B12 would alleviate DTT toxicity in the hypoxia response pathway mutants. While the supplementation of 50 nM vitamin B12 alleviated DTT toxicity in wild-type N2 animals, it failed to do so in the hypoxia response pathway mutants (Figures 4E and 4F). Similarly, the wild-type animals developed on 10 mM DTT in the presence of the bacterial diet *Comamonas aquatica* DA1877, which has higher vitamin B12 compared to the *E. coli* OP50 diet (Gokul and Singh, 2022; Watson et al., 2014), while the hypoxia response pathway mutants failed to develop (Figures S4A and S4B). Taken together, these results indicated that the hypoxia response pathway protects against thiol reductive stress.

Activation of the hypoxia response pathway by thiol reductive stress is conserved in human cell lines

Next, we asked whether the activation of the hypoxia response pathway by thiol reductive stress is a conserved response. To this end, we used three human cell lines from different tissue origins, including HeLa (cervical cancer), LN229 (glioblastoma), and Cal27 (oral squamous cell carcinoma). We exposed these cell lines to 10 mM DTT for 24 hours and evaluated the mRNA levels of five hypoxia-response genes, including hypoxia-inducible factor-1*α* (*HIF-1α)*, *HIF-1β*, 3-phosphoinositide-dependent protein kinase-1 (*PDK1)*, glucose transporter 1 *(GLUT1)*, and BCL2/adenovirus E1B 19 kDa protein-interacting protein 3 (*BNIP3)*. All of these genes are known to be upregulated under hypoxic conditions (BelAiba

et al., 2007; Choudhry and Harris, 2018; Guo et al., 2001). DTT treatment also resulted in the upregulation of these genes in HeLa, LN229, and Cal27 cell lines (Figures 5A-5C). These results showed that thiol reductive stress activates the hypoxia response pathway in human cell lines.

Thiol reductive stress depletes cellular oxygen

Finally, we asked how thiol reductive stress leads to the activation of the hypoxia response pathway. Thiol antioxidants result in the breakage of disulfide bonds in the ER (Maity et al., 2016). This is followed by the activation of futile oxidative cycles in the ER, enhancing disulfide bond turnover (Maity et al., 2016). Disulfide bond formation consumes oxygen and produces hydrogen peroxide (Zito, 2015). Therefore, thiol reductive stress generates hydrogen peroxide and causes oxidative stress (Maity et al., 2016). We hypothesized that thiol reductive stress might activate the hypoxia response pathway by creating oxidative stress or directly enhancing oxygen consumption. To delineate between these two possibilities, we knocked down *ero-1* and studied DTT-mediated *rips-1* induction. The gene *ero-1* encodes for a protein disulfide oxidase that is involved in disulfide bond formation in the ER and generates hydrogen peroxide in the process (Zito, 2015). Knockdown of *ero-1* did not affect *rips-1* expression levels in the absence and presence of DTT (Figures 6A and 6B). Because disulfide bond formation and hydrogen peroxide production also occur by *ero-1*-independent mechanisms (Konno et al., 2015), we directly probed the role of oxidative stress in the upregulation of *rips-1*. While oxidative stress by tert-butyl hydroperoxide, ferric chloride, and paraquat resulted in the induction of oxidative stress reporter *gst-4p::GFP*, it did not affect the expression of *rips-1p::GFP* (Figures S5A and S5B). These results suggested that oxidative stress does not activate the hypoxia response pathway.

Next, we tested whether thiol reductive stress resulted in the consumption of oxygen to hypoxia levels. To this end, we stained human cell lines with Image-iT green hypoxia reagent after treatment with 10 mM DTT. Image-iT green hypoxia reagent is a fluorogenic compound that is live cell permeable and senses oxygen levels. It becomes fluorescent only when oxygen levels reach below 5%, and the fluorescence signal increases with declining oxygen concentrations. DTT treatment resulted in a drastic increase in fluorescence in HeLa, LN229, and Cal27 cell lines (Figures 6C-6F), indicating low-oxygen environments in the

cells. Taken together, these results indicated that thiol reductive stress creates hypoxia and activates the hypoxia response pathway by enhancing oxygen consumption.

Discussion

Despite links with various pathological conditions, the physiological effects of reductive stress remain poorly characterized (Handy and Loscalzo, 2017; Ma et al., 2020; Pérez-Torres et al., 2017; Rajasekaran, 2020). In this study, we show that thiol reductive stress creates hypoxia by enhancing cellular oxygen consumption and activates the hypoxia response pathway. The hypoxia response pathway appears to be protective against reductive stress as mutants defective in activating the hypoxia response pathway have increased sensitivity to DTT. Hypoxia has been shown to protect against mitochondrial reductive stress by enhancing the production of L-2-hydroxyglutarate (Oldham et al., 2015). The hypoxia response pathway also enhances the catabolism of hydrogen sulfide (H_2S) by enhancing the expression of sulfide:quinone oxidoreductase (Budde and Roth, 2011; Malagrinò et al., 2019). H_2S is a strong reducing agent and likely causes thiol reductive stress (Giuffrè and Vicente, 2018; Hanna et al., 2023). Therefore, the hypoxia response pathway appears to have evolved to defend against reductive stress.

Disulfide bond formation occurs by multiple mechanisms in eukaryotic cells (Bulleid and Ellgaard, 2011). In yeast, *ero-1* is an essential gene because it encodes for the major enzyme involved in disulfide bond formation (Frand and Kaiser, 1998; Pollard et al., 1998). However, in higher eukaryotes, multiple mechanisms of disulfide bond formation occur, and *ero-1* is not an essential gene (Bulleid and Ellgaard, 2011). Regardless of the type of enzymatic system involved, oxygen consumption is a common feature of disulfide bond formation (Bulleid and Ellgaard, 2011). Therefore, the increased disulfide bond turnover under reducing conditions enhances the consumption of cellular oxygen. The oxidation of thiol groups also generates oxidative stress by producing hydrogen peroxide (Maity et al., 2016; Netto and Stadtman, 1996). However, we observed that oxidative stress does not activate the hypoxia response pathway. After thiol reductive stress, the ER steady-state disulfide content is restored on a time scale of seconds (Appenzeller-herzog et al., 2010). Because of the very rapid kinetics of disulfide bond formation, thiol reductive stress could result in the consumption of large amounts of cellular oxygen. Therefore, it appears that the

consumption of cellular oxygen by enhanced disulfide bond turnover is the likely cause of hypoxia under thiol reductive stress.

Because disulfide bond formation involves oxygen consumption in all aerobic organisms (Sevier and Kaiser, 2002), thiol reductive stress is expected to induce hypoxia in diverse organisms. Indeed, we find that induction of hypoxia by thiol reductive stress is conserved in *C. elegans* and multiple human cell lines. Several cell types, such as plasma cells, goblet cells, and pancreatic acinar cells, are involved in the secretion of a large number of disulfide-bonded proteins. An active plasma cell is estimated to form 10^5 disulfide bonds per second (Bertolotti et al., 2010). Such a high rate of disulfide bond formation is likely to create hypoxia in professional secretory cells. Therefore, the hypoxia response pathway might have evolved to improve the efficiency of the secretory pathway. Indeed, hypoxia enhances the expression of *ERO1* in human, rat, and mouse cells (Gess et al., 2003), and likely augments disulfide bond formation in the ER.

The endogenously produced signaling molecule H_2S provides cytoprotection by activating the hypoxia response pathway (Blackstone and Roth, 2007; Budde and Roth, 2010; Miller and Roth, 2007). However, the mechanism of activation of the hypoxia response pathway by this molecule is not well understood. It is believed that H_2S activates the hypoxia response pathway by inhibiting oxygen consumption by mitochondrial cytochrome oxidase (Cooper and Brown, 2008). However, H_2S also causes thiol reductive stress because of its strong reducing potential (Giuffrè and Vicente, 2018; Hanna et al., 2023). Therefore, activation of the hypoxia response pathway by H_2S could also be mediated because of the ensuing thiol reductive stress. Indeed, H_2S has been shown to enhance oxygen consumption in chicken liver cells (Yong and Searcy, 2001). In future studies, it will be intriguing to test the relative contribution of cytochrome oxidase inhibition and thiol reductive stress in the activation of the hypoxia response by H_2S.

The hypoxia response pathway has important roles in health, lifespan, and various pathological conditions. Mice with constitute active hypoxia response pathway are protected against a myriad of pathological conditions, including obesity and metabolic dysfunction (Rahtu-Korpela et al., 2014), cardiac and skeletal muscle ischemia (Hassinen et al., 2010; Karsikas et al., 2016), cardiac hypertrophy (Roning et al., 2022), atherosclerosis (Rahtu-korpela et al., 2016), and alcoholic fatty liver diseases (Laitakari et al., 2019). Activation of the hypoxia response pathway under normoxia conditions increases stress resistance (Bellier

et al., 2009), reduces susceptibility to neurodegenerative disease, and increases lifespan (Mehta et al., 2009) in *C. elegans*. Even intermittent exposure to hypoxic conditions drastically enhances *C. elegans* lifespan (Pitt et al., 2022; Schieber and Chandel, 2014). Because activation of the hypoxia response pathway confers several health-promoting and lifespan-improving effects, small molecules that activate the hypoxia response pathway could provide therapeutic intervention points to improve health and lifespan (Nagle and Zhou, 2006). In the current study, we discover that DTT activates the hypoxia response pathway. DTT is known to attenuate several pathological conditions, including hepatic, hematopoietic, intestinal, and renal injuries (Heidari et al., 2016, 2018; Li et al., 2019). However, it is not known whether these effects of DTT are via the hypoxia response pathway or sequestration of ROS. It will be intriguing to test whether hormetic thiol reductive stress could have health and lifespan-improving effects via the hypoxia response pathway.

Materials and Methods

Bacterial strains

The following bacterial strains were used in the current study: *Escherichia coli* OP50, *E. coli* HT115(DE3), *Pseudomonas aeruginosa* PAO1, and *Comamonas aquatica* DA1877. The cultures of *E. coli* OP50, *E. coli* HT115(DE3), and *C. aquatica* DA1877 were grown in Luria-Bertani (LB) broth at 37°C. The *P. aeruginosa* PAO1 cultures were grown in brain heart infusion (BHI) broth at 37°C.

C. elegans strains and growth conditions

C. elegans hermaphrodites were maintained at 20°C on nematode growth medium (NGM) plates seeded with *E. coli* OP50 as the food source unless otherwise indicated. Bristol N2 was used as the wild-type control unless otherwise indicated. The following strains were used in the study: JSJ13 *jsnIs1[rips-1p::GFP + myo-2p::mCherry]*, ZG31 *hif-1(ia4)*, ZG120 *unc-119(ed3);iaIs7[nhr-57p::GFP + unc-119(+)]*, and CL2166 *dvIs19[(pAF15)gst-4p::GFP::NLS]*. The following strains were generated in this study: JSJ14 *jsnIs1[rips-1p::GFP + myo-2p::mCherry];rhy-1(jsn13);rhy-1(jsn14)*, JSJ15 *jsnIs1[rips-1p::GFP + myo-2p::mCherry];egl-9(jsn15)*, JSJ16 *jsnIs1[rips-1p::GFP + myo-2p::mCherry];vhl-1(jsn16)*, JSJ17 *jsnIs1[rips-1p::GFP + myo-2p::mCherry];cysl-1(jsn17)*, and JSJ18 *jsnIs1[rips-1p::GFP + myo-2p::mCherry];cysl-1(jsn18)*. Some of the strains were obtained from the

Caenorhabditis Genetics Center (University of Minnesota, Minneapolis, MN). The *hif-1(ia4);rips-1p::GFP* strain was obtained by standard genetic crosses.

Preparation of NGM plates with different supplements

The following supplements with their product numbers were obtained from HiMedia BioSciences: DTT (#RM525), vitamin B12 (cyanocobalamin) (#PCT0204), ferric chloride (#TC583), and tert-butyl hydroperoxide (#RM2022). Paraquat was obtained from Sigma-Aldrich (#856177). The supplements were added to the nematode growth media just before pouring them into plates to obtain the desired final concentration.

***C. elegans* development assays**

Synchronized *C. elegans* eggs were obtained by transferring 20-25 gravid adult hermaphrodites on NGM plates for egg-laying for 2 hours. After 2 hours, the gravid adults were removed. The synchronized eggs were incubated at 20°C for 72 hours. After that, the animals in different development stages (L1/L2, L3, and L4/adult) were quantified. Representative images of the NGM plates at the time of quantification of development were also captured. At least three independent experiments (biological replicates) were performed for each condition.

RNA interference (RNAi)

RNAi was used to generate loss-of-function RNAi phenotypes by feeding worms with *E. coli* HT115(DE3) expressing double-stranded RNA homologous to a target *C. elegans* gene. *E. coli* with the appropriate vectors were grown in LB broth containing ampicillin (100 μg/mL) at 37°C overnight and plated onto RNAi NGM plates containing 100 μg/mL ampicillin and 3 mM isopropyl β-D-thiogalactoside (IPTG). The RNAi-expressing bacteria were allowed to grow overnight at 37°C on RNAi plates without DTT. On the other hand, the RNAi plates with 10 mM DTT were kept at room temperature for 2 days upon seeding with bacterial cultures. The worms were synchronized on RNAi plates, and the eggs were allowed to develop at 20°C for 72 hours. The RNAi clones were from the Ahringer RNAi library and were verified by sequencing.

Forward genetic screens for mutants with upregulated *rips-1p::GFP* expression levels

Ethyl methanesulfonate (EMS) mutagenesis screens (Singh, 2021) were performed using the *rips-1p::GFP* strain. Approximately 2500 synchronized late L4 larvae were treated with 50 mM EMS for 4 hours and then washed three times with M9 medium. The washed animals (P0 generation) were then transferred to 9-cm NGM plates containing *E. coli* OP50 and allowed to lay eggs (F1 progeny) overnight. The P0s were then washed away with M9 medium, while the F1 eggs remained attached to the bacterial lawn. The F1 eggs were allowed to grow to adulthood. The adult F1 animals were bleached to obtain F2 eggs. The F2 eggs were transferred to *E. coli* OP50 plates containing 50 nM vitamin B12 and incubated at 20°C for 72 hours. After that, the plates were screened for animals that had high GFP levels. Approximately 50,000 haploid genomes were screened, and three mutants were isolated. All of the mutants were backcrossed six times with the parental *rips-1p::GFP* strain before analysis.

Forward genetic screens for mutants that lacked DTT-mediated *rips-1p::GFP* upregulation

All the mutagenesis steps were identical with the screen for mutants with upregulated *rips-1p::GFP* expression levels until the F2 eggs stage. The F2 eggs were transferred to *E. coli* OP50 plates and incubated at 20°C for 72 hours. After that, the adult F2 animals were washed away with M9 and transferred to *E. coli* OP50 plates containing 10 mM DTT. After 10 hours of incubation, the plates were screened for animals that lacked GFP induction. Approximately 50,000 haploid genomes were screened, and two mutants were isolated. Both the mutants were backcrossed six times with the parental *rips-1p::GFP* strain before analysis.

Whole-genome sequencing (WGS) and data analysis

The genomic DNA was isolated as described earlier (Gokul and Singh, 2022; Singh and Aballay, 2017). Briefly, the mutant animals were grown at 20°C on NGM plates seeded with *E. coli* OP50 until starvation. Four 9-cm *E. coli* OP50 plates were used for each strain to obtain a sufficient number of animals. The animals were rinsed off the plates with M9, washed three times, incubated in M9 with rotation for 2 hours to eliminate food from the intestine, and washed three times again with distilled water, followed by storage at -80°C

until genomic DNA extraction. Genomic DNA extraction was performed using the Gentra Puregene Kit (Qiagen, Netherlands). DNA libraries were prepared according to a standard Illumina (San Diego, CA) protocol. The DNA was subjected to WGS on an Illumina NovaSeq 6000 sequencing platform using 150 paired-end nucleotide reads. Library preparation and WGS were performed at the National Genomics Core, National Institute of Biomedical Genomics, Kalyani, India.

The whole-genome sequence data were analyzed using the web platform Galaxy as described earlier (Gokul and Singh, 2022). Briefly, the forward and reverse FASTQ reads, *C. elegans* reference genome Fasta file (ce11M.fa), and the gene annotation file (SnpEff4.3 WBcel235.86) were input into the Galaxy workflow. The low-quality ends of the FASTQ reads were trimmed using the Sickle tool. The trimmed FASTQ reads were mapped to the reference genome Fasta files with the BWA-MEM tool. Using the MarkDuplicates tool, any duplicate reads (mapped to multiple sites) were filtered. Subsequently, the variants were detected using the FreeBayes tool that finds small polymorphisms, including single-nucleotide polymorphisms (SNPs), insertions and deletions (indels), multi-nucleotide polymorphisms (MNPs), and complex events (composite insertion and substitution events) smaller than the length of a short-read sequencing alignment. The common variants among different mutants were subtracted. The SnpEff4.3 WBcel235.86 gene annotation file was used to annotate and predict the effects of genetic variants (such as amino acid changes). Finally, the linkage maps for each mutant were generated using the obtained variations.

C. elegans RNA isolation and quantitative reverse transcription-PCR (qRT-PCR)

Animals were synchronized by egg laying. Approximately 40 gravid adult animals were transferred to 9-cm *E. coli* OP50 plates without DTT and allowed to lay eggs for 4 hours. The gravid adults were then removed, and the eggs were allowed to develop at 20°C for 72 hours. Subsequently, the synchronized adult animals were collected with M9, washed twice with M9, and then transferred to 9-cm *E. coli* OP50 plates containing 10 mM DTT. The control animals were maintained on *E. coli* OP50 plates without DTT. After the transfer of the animals, the plates were incubated at 20°C for 10 hours. Subsequently, the animals were collected, washed with M9 buffer, and frozen in TRIzol reagent (Life Technologies, Carlsbad, CA). Total RNA was extracted using the RNeasy Plus Universal Kit (Qiagen, Netherlands). A total of 1 μg of total RNA was reverse-transcribed with random primers

using the PrimeScript™ 1st strand cDNA Synthesis Kit (TaKaRa) according to the manufacturer's protocols. qRT-PCR was conducted using TB Green fluorescence (TaKaRa) on a LightCycler 480 II System (Roche Diagnostics) in 96-well-plate format. Twenty microliter reactions were analyzed as outlined by the manufacturer (TaKaRa). The relative fold-changes of the transcripts were calculated using the comparative $CT(2^{-\Delta\Delta CT})$ method and normalized to pan-actin (*act-1, -3, -4*) as described earlier (Singh and Aballay, 2019a). All samples were run in triplicate and repeated at least three times.

Fast-killing assays on *P. aeruginosa* PAO1

For fast-killing assays, *P. aeruginosa* PAO1 cultures were grown by inoculating individual bacterial colonies into 4-5 mL of BHI broth and incubated for 10–12 hours on a shaker at 37°C. Then, the cultures were diluted ten times in BHI broth, and 50 μL of the diluted culture was spread on a 3.5-cm BHI agar plate. After spreading bacteria, plates were incubated at 37°C for 24 hours. After that, the plates were allowed to cool to room temperature, and worms synchronized on NGM plates seeded with *C. aquatica* DA1877 with and without 5 mM DTT at the L4 stage were transferred to them. Plates were kept at room temperature and scored for live and dead worms at indicated times of transfer.

Impact of oxidative stress on *rips-1p::GFP* expression

Egg laying of *rips-1p::GFP* and *gst-4p::GFP* animals was carried out by transferring gravid adult hermaphrodites on NGM plates seeded with *E. coli* OP50 for 4 hours. Worms were removed after egg laying, and the plates containing eggs were incubated at 20°C. After 72 hours, synchronized adult worms were transferred to *E. coli* OP50 plates containing 1 mM paraquat, 5 mM tert-butyl hydroperoxide, and 7.5 mM ferric chloride for 12 hours. After that, the animals were prepared for fluorescence imaging.

***nhr-57p::GFP* induction assays**

The *nhr-57p::GFP* animals were synchronized by egg laying on *E. coli* OP50 plates without DTT and incubated at 20°C for 72 hours. Subsequently, the animals were transferred to *E. coli* OP50 plates containing 0 and 10 mM DTT and incubated at 20°C for 10 hours. After that, the animals were prepared for fluorescence imaging.

Fluorescence imaging of *C. elegans*

Fluorescence imaging was carried out as described previously (Gokul and Singh, 2022; Singh and Aballay, 2019b). Briefly, the animals were anesthetized using an M9 salt solution containing 50 mM sodium azide and mounted onto 2% agarose pads. The animals were then visualized using a Nikon SMZ-1000 fluorescence stereomicroscope. The fluorescence intensity was quantified using Image J software.

Cell culture

Human cell lines, HeLa (cervical cancer), LN229 (glioblastoma), and Cal27 (oral squamous cell carcinoma), were obtained from the National Center of Cell Science (NCCS), Pune. The cells were cultured in a humidified incubator at 37°C and 5% CO_2 in Dulbecco's modified eagle medium (DMEM), supplemented with 10% fetal bovine serum. The culture medium was replenished every third day. The study with human cell lines was approved by the institute ethics committee, PGIMER, with approval number IEC-01/2023-2648.

Cell lines RNA isolation and qRT-PCR

HeLa, LN229, and Cal27 cell lines were treated with 10 mM DTT for 24 hours. The total RNA of DTT treated and control cells was isolated using the TRIzol method. Total RNA was reverse transcribed to cDNA using the High-Capacity cDNA Reverse Transcription Kit (Applied Biosystems), as per the manufacturer's instructions. qRT-PCR was conducted using DyNAmo ColorFlash SYBR Green (ThermoFisher Scientific) on a CFX96 Real-Time System (Bio-Rad) in 96-well-plate format. Twenty microliter reactions were analyzed as outlined by the manufacturer (Bio-Rad). The relative fold changes of the transcripts were calculated using the comparative $CT(2^{-\Delta\Delta CT})$ method and normalized to beta-actin. All samples were run in triplicate and repeated at least three times.

Hypoxia staining of human cell lines and quantification

Human cell lines were pretreated with 10 mM DTT for 24 hours. After that, the cells were treated with Image-iT™ Green Hypoxia Reagent (Invitrogen) at a concentration of 1 µM for 30 minutes at 37ºC. The reagent was then removed, and the cells were incubated in either DMEM (control) or DMEM containing 10 mm DTT for 4 hours. After that, cell images were captured using a fluorescence microscope (Leica) at the excitation/emission wavelength of 488/520 nm. Simultaneously, cells were separately cultured in 96-well plates and stained with the Image-iT™ Green Hypoxia Reagent as described above. The fluorescence of the cells was then read in a fluorescence plate reader (Infinite 200 Pro, TECAN) at the

excitation/emission wavelengths of FITC (488/520 nm) with the following parameters: Z-position 20000 µm, gain 100, excitation bandwidth 9 nm, emission bandwidth 20 nm, and the number of flashes 25.

Quantification and Statistical Analysis

The statistical analysis was performed with Prism 8 (GraphPad). All error bars represent mean±standard deviation (SD). The two-sample *t*-test was used when needed, and the data were judged to be statistically significant when $p < 0.05$. In the figures, asterisks (*) denote statistical significance as follows: *, $p < 0.05$, **, $p < 0.01$, ***, $p < 0.001$, as compared with the appropriate controls.

Supplemental information

The supplemental information includes five figures and a table.

Data Availability: The whole-genome sequence data for JSJ14-JSJ18 have been submitted to the public repository, the Sequence Read Archive, with BioProject ID PRJNA933286. All data generated or analyzed during this study are included in the manuscript and supporting files.

Acknowledgments

Some strains used in this study were provided by the Caenorhabditis Genetics Center (CGC), which is funded by the NIH Office of Research Infrastructure Programs (P40 OD010440). We thank Shweta Saini (IISER Mohali) for assistance with *C. elegans* forward genetic screens and Aditi Bhagat (PGIMER Chandigarh) for assistance with cell culture experiments.

Funding: This work was supported by the Ramalingaswami Re-entry Fellowship (Ref. No. BT/RLF/Re-entry/50/2020) awarded by the Department of Biotechnology, India, Science and Engineering Research Board (SERB) Startup Research Grant (Ref. No. SRG/2020/000022) awarded by DST, India, and IISER Mohali intramural funds.

Author contributions

Ravi and J.S. conceived and designed the study; Ravi performed the *C. elegans* experiments; Ravi and J.S. analyzed and interpreted the *C. elegans* data; A.K. planned, performed, and analyzed human cell line experiments; S.B. supervised human cell line experiments; J.S. wrote the manuscript with inputs from Ravi and A.K.

Declaration of interests: The authors declare that they have no competing interests.

References

Appenzeller-herzog, C., Riemer, J., Zito, E., Chin, K.-T., Ron, D., Spiess, M., and Ellgaard, L. (2010). Disulphide production by Ero1a–PDI relay is rapid and effectively regulated. EMBO J. *29*, 3318–3329.

Ates, I., Kaplan, M., Yuksel, M., Mese, D., Alisik, M., Erel, O., Yilmaz, N., and Guler, S. (2016). Determination of thiol / disulphide homeostasis in type 1 diabetes mellitus and the factors associated with thiol oxidation. Endocrine *51*, 47–51.

BelAiba, R.S., Bonello, S., Zahringer, C., Schmidt, S., Hess, J., Kietzmann, T., and Gorlach, A. (2007). Hypoxia Up-Regulates Hypoxia-Inducible Factor-1a Transcription by Involving Phosphatidylinositol 3-Kinase and Nuclear Factor kB in Pulmonary Artery Smooth Muscle Cells. Mol. Biol. Cell *18*, 4691–4697.

Bellier, A., Chen, C.S., Kao, C.Y., Cinar, H.N., and Aroian, R. V. (2009). Hypoxia and the hypoxic response pathway protect against pore-forming toxins in C. elegans. PLoS Pathog. *5*, e1000689.

Bertolotti, M., Yim, S.H., Garcia-Manteiga, J.M., Masciarelli, S., Kim, Y.-J., Kang, M.-H., Iuchi, Y., Fujii, J., Vene, R., Rubartelli, A., et al. (2010). B- to Plasma-Cell Terminal Differentiation Entails Oxidative Stress and Profound Reshaping of the Antioxidant Responses. Antioxid. Redox Signal. *13*, 1133–1144.

Blackstone, E., and Roth, M.B. (2007). Suspended animation-like state protects mice from lethal hypoxia. Shock *27*, 370–372.

Braakman, I., Helenius, J., and Helenius, A. (1992). Manipulating disulfide bond formation and protein folding in the endoplasmic reticulum. EMBO J. *11*, 1717–1722.

Budde, M.W., and Roth, M.B. (2010). Hydrogen Sulfide Increases Hypoxia-inducible Factor-1 Activity Independently of von Hippel–Lindau Tumor Suppressor-1 in C. elegans. Mol. Biol. Cell *21*, 212–217.

Budde, M.W., and Roth, M.B. (2011). The response of caenorhabditis elegans to Hydrogen Sulfide and Hydrogen Cyanide. Genetics *189*, 521–532.

Bulleid, N.J., and Ellgaard, L. (2011). Multiple ways to make disulfides. Trends Biochem. Sci. *36*, 485–492.
Choudhry, H., and Harris, A.L. (2018). Advances in Hypoxia-Inducible Factor Biology. Cell Metab. *27*, 281–298.
Cooper, C.E., and Brown, G.C. (2008). The inhibition of mitochondrial cytochrome oxidase by the gases carbon monoxide, nitric oxide, hydrogen cyanide and hydrogen sulfide: Chemical mechanism and physiological significance. J. Bioenerg. Biomembr. *40*, 533–539.
Cuozzo, J.W., and Kaiser, C.A. (1999). Competition between glutathione and protein thiols for disulphide-bond formation. Nat. Cell Biol. *1*, 130–135.
Doering, K.R.S., Cheng, X., Milburn, L., Ratnappan, R., Ghazi, A., Miller, D.L., and Taubert, S. (2022). Nuclear hormone receptor NHR-49 acts in parallel with HIF-1 to promote hypoxia adaptation in Caenorhabditis elegans. Elife *11*, e67911.
Epstein, A.C.R., Gleadle, J.M., McNeill, L.A., Hewitson, K.S., O'Rourke, J., Mole, D.R., Mukherji, M., Metzen, E., Wilson, M.I., Dhanda, A., et al. (2001). C. elegans EGL-9 and mammalian homologs define a family of dioxygenases that regulate HIF by prolyl hydroxylation. Cell *107*, 43–54.
Frand, A.R., and Kaiser, C.A. (1998). The ERO1 gene of yeast is required for oxidation of protein dithiols in the endoplasmic reticulum. Mol. Cell *1*, 161–170.
Gallagher, L.A., and Manoil, C. (2001). Pseudomonas aeruginosa PAO1 Kills Caenorhabditis elegans by Cyanide Poisoning. J. Bacteriol. *183*, 6207–6214.
Gess, B., Hofbauer, K., Wenger, R.H., Lohaus, C., Meyer, H.E., and Kurtz, A. (2003). The cellular oxygen tension regulates expression of the endoplasmic oxidoreductase ERO1-L a. Eur. J. Biochem. *270*, 2228–2235.
Giuffrè, A., and Vicente, J.B. (2018). Hydrogen sulfide biochemistry and interplay with other gaseous mediators in mammalian physiology. Oxid. Med. Cell. Longev. *2018*, 6290931.
Gokul, G., and Singh, J. (2022). Dithiothreitol causes toxicity in C. elegans by modulating the methionine-homocysteine cycle. Elife *11*, e76021.
Guo, K., Searfoss, G., Krolikowski, D., Pagnoni, M., Franks, C., Clark, K., Yu, K.T., Jaye, M., and Ivashchenko, Y. (2001). Hypoxia induces the expression of the pro-apoptotic gene BNIP3. Cell Death Differ. *8*, 367–376.
Gusarov, I., Shamovsky, I., Pani, B., Gautier, L., Eremina, S., Katkova-Zhukotskaya, O., Mironov, A., Makarov, A., and Nudler, E. (2021). Dietary thiols accelerate aging of C. elegans. Nat. Commun. *12*, 4336.
Handy, D.E., and Loscalzo, J. (2017). Responses to reductive stress in the cardiovascular

system. Free Radic. Biol. Med. *109*, 114–124.
Hanna, D., Kumar, R., and Banerjee, R. (2023). A Metabolic Paradigm for Hydrogen Sulfide Signaling via Electron Transport Chain Plasticity. Antioxid. Redox Signal. *38*, 57–67.
Hassinen, I.E., Sormunen, R., Ma, J.M., Kivirikko, K.I., Koivunen, P., and Myllyharju, J. (2010). Hearts of Hypoxia-inducible Factor Prolyl 4-Hydroxylase-2 Hypomorphic Mice Show Protection against Acute Ischemia-Reperfusion Injury. J. Biol. Chem. *285*, 13646–13657.
Heidari, R., Taheri, V., Rahimi, H.R., Yeganeh, B.S., Niknahad, H., and Najibi, A. (2016). Sulfasalazine-induced renal injury in rats and the protective role of thiol-reductants. Ren. Fail. *38*, 137–141.
Heidari, R., Ghanbarinejad, V., Mohammadi, H., Ahmadi, A., Esfandiari, A., Azarpira, N., and Niknahad, H. (2018). Dithiothreitol supplementation mitigates hepatic and renal injury in bile duct ligated mice: Potential application in the treatment of cholestasis-associated complications. Biomed. Pharmacother. *99*, 1022–1032.
Karsikas, S., Myllymäki, M., Heikkilä, M., Sormunen, R., Kivirikko, K.I., Myllyharju, J., Serpi, R., and Koivunen, P. (2016). HIF-P4H-2 deficiency protects against skeletal muscle ischemia-reperfusion injury. J. Mol. Med. *94*, 301–310.
Konno, T., Melo, E.P., Lopes, C., Mehmeti, I., Lenzen, S., Ron, D., and Avezov, E. (2015). ERO1-independent production of H2O2 within the endoplasmic reticulum fuels Prdx4-mediated oxidative protein folding. J. Cell Biol. *211*, 253–259.
Kundi, H., Ates, I., Kiziltunc, E., Cetin, M., Cicekcioglu, H., Neselioglu, S., Erel, O., and Ornek, E. (2015). A Novel Oxidative Stress Marker In Acute Myocardial Infarction; Thiol/ Disulphide Homeostasis. Am. J. Emerg. Med. *33*, 1567–1571.
Laitakari, A., Ollonen, T., Kietzmann, T., Walkinshaw, G., Mennerich, D., Izzi, V., Haapasaari, K., Myllyharju, J., Serpi, R., Dimova, E.Y., et al. (2019). Systemic inactivation of hypoxia-inducible factor prolyl 4-hydroxylase 2 in mice protects from alcohol-induced fatty liver disease. Redox Biol. *22*, 101145.
Li, K., Zhang, J., Cao, J., Li, X., and Tian, H. (2019). 1,4-Dithiothreitol treatment ameliorates hematopoietic and intestinal injury in irradiated mice: Potential application of a treatment for acute radiation syndrome. Int. Immunopharmacol. *76*, 105913.
Ma, D.K., Vozdek, R., Bhatla, N., and Horvitz, H.R. (2012). CYSL-1 Interacts with the O 2-Sensing Hydroxylase EGL-9 to Promote H 2S-Modulated Hypoxia-Induced Behavioral Plasticity in C. elegans. Neuron *73*, 925–940.
Ma, W.X., Li, C.Y., Tao, R., Wang, X.P., and Yan, L.J. (2020). Reductive Stress-Induced

Mitochondrial Dysfunction and Cardiomyopathy. Oxid. Med. Cell. Longev. *2020*.
Maity, S., Rajkumar, A., Matai, L., Bhat, A., Ghosh, A., Agam, G., Kaur, S., Bhatt, N.R., Mukhopadhyay, A., Sengupta, S., et al. (2016). Oxidative Homeostasis Regulates the Response to Reductive Endoplasmic Reticulum Stress through Article Oxidative Homeostasis Regulates the Response to Reductive Endoplasmic Reticulum Stress through Translation Control. Cell Rep. *16*, 851–865.
Malagrinò, F., Zuhra, K., Mascolo, L., Mastronicola, D., Vicente, J.B., Forte, E., and Giuffrè, A. (2019). Hydrogen sulfide oxidation: Adaptive changes in mitochondria of SW480 colorectal cancer cells upon exposure to hypoxia. Oxid. Med. Cell. Longev. *2019*, 8102936.
Mehta, R., Steinkraus, K. a, Sutphin, G.L., Ramos, F.J., Shamieh, L.S., Huh, A., Davis, C., Chandler-brown, D., and Kaeberlein, M. (2009). Proteasomal Regulation of the Hypoxic Response Modulates Aging in C. elegans. Science (80-.). *324*, 1196–1198.
Merksamer, P.I., Trusina, A., and Papa, F.R. (2008). Real-Time Redox Measurements during Endoplasmic Reticulum Stress Reveal Interlinked Protein Folding Functions. Cell *135*, 933–947.
Miller, D.L., and Roth, M.B. (2007). Hydrogen sulfide increases thermotolerance and lifespan in Caenorhabditis elegans. Proc. Natl. Acad. Sci. U. S. A. *104*, 20618–20622.
Nagle, D.G., and Zhou, Y. (2006). Natural Product-Derived Small Molecule Activators of Hypoxia-Inducible Factor-1 (HIF-1). Curr. Pharm. Des. *12*, 2673–2688.
Netto, L.E.S., and Stadtman, E.R. (1996). The Iron-Catalyzed Oxidation of Dithiothreitol Is a Biphasic Process: Hydrogen Peroxide Is Involved in the Initiation of a Free Radical Chain of Reactions. Arch. Biochem. Biophys. *333*, 233–242.
Oldham, W.M., Clish, C.B., Yang, Y., and Loscalzo, J. (2015). Hypoxia-Mediated Increases in L-2-hydroxyglutarate Coordinate the Metabolic Response to Reductive Stress. Cell Metab. *22*, 291–303.
Oslowski, C.M., and Urano, F. (2011). Measuring ER Stress and the Unfolded Protein Response Using Mammalian Tissue Culture System. Methods Enzymol. *490*, 71–92.
Pérez-Torres, I., Guarner-Lans, V., and Rubio-Ruiz, M.E. (2017). Reductive stress in inflammation-associated diseases and the pro-oxidant effect of antioxidant agents. Int. J. Mol. Sci. *18*, 1–26.
Pitt, J.N., Chavez, E., Provencher, K.M., Chen, M., Tran, C., Tran, J., Huang, K., Vaid, A., Abadir, M.L., Arang, N., et al. (2022). Intermittent hypoxia therapy engages multiple longevity pathways to double lifespan in C. elegans. BioRxiv doi.org/10.1101/2022.10.13.512140.

Pollard, M.G., Travers, K.J., and Weissman, J.S. (1998). Ero1p: A novel and ubiquitous protein with an essential role in oxidative protein folding in the endoplasmic reticulum. Mol. Cell *1*, 171–182.

Rahtu-korpela, L., Määttä, J., Dimova, E.Y., Hörkkö, S., Gylling, H., Walkinshaw, G., Hakkola, J., Kivirikko, K.I., Myllyharju, J., Serpi, R., et al. (2016). Hypoxia-Inducible Factor Prolyl 4-Hydroxylase-2 Inhibition Protects Against Development of Atherosclerosis. Arterioscler. Thromb. Vasc. Biol. *36*, 608–617.

Rahtu-Korpela, L., Karsikas, S., Hörkkö, S., Sequeiros, R.B., Lammentausta, E., Mäkelä, K.A., Herzig, K., Walkinshaw, G., Kivirikko, K.I., Myllyharju, J., et al. (2014). HIF Prolyl 4-Hydroxylase-2 Inhibition Improves Glucose and Lipid Metabolism and Protects Against Obesity and Metabolic Dysfunction. Diabetes *63*, 3324–3333.

Rajasekaran, N.-S. (2020). Reductive Stress: Neglected Science. Antioxid. Redox Signal. *32*, 8114.

Rodrigues, S.D., Batista, G.B., Ingberman, M., Pecoits-Filho, R., and Nakao, L.S. (2013). Plasma cysteine/cystine reduction potential correlates with plasma creatinine levels in chronic kidney disease. Blood Purif. *34*, 231–237.

Roning, T., Magga, J., Laitakari, A., Halmetoja, R., Tapio, J., Dimova, E.Y., Szabo, Z., Rahtu-korpela, L., Kemppi, A., Walkinshaw, G., et al. (2022). Activation of the hypoxia response pathway protects against age-induced cardiac hypertrophy. J. Mol. Cell. Cardiol. *164*, 148–155.

Sayin, V.I., Ibrahim, M.X., Larsson, E., Nilsson, J.A., Lindahl, P., and Bergo, M.O. (2014). Antioxidants accelerate lung cancer progression in mice. Sci. Transl. Med. *6*, 221ra15.

Schieber, M., and Chandel, N.S. (2014). TOR signaling couples oxygen sensing to lifespan in C.elegans. Cell Rep. *9*, 9–15.

Sevier, C.S., and Kaiser, C.A. (2002). Formation and transfer of disulphide bonds in living cells. Nat. Rev. Mol. Cell Biol. *3*, 836–847.

Shen, C., Nettleton, D., Jiang, M., Kim, S.K., and Powell-Coffman, J.A. (2005). Roles of the HIF-1 hypoxia-inducible factor during hypoxia response in Caenorhabditis elegans. J. Biol. Chem. *280*, 20580–20588.

Shen, C., Shao, Z., and Powell-Coffman, J.A. (2006). The Caenorhabditis elegans rhy-1 gene inhibits HIF-1 hypoxia-inducible factor activity in a negative feedback loop that does not include vhl-1. Genetics *174*, 1205–1214.

Sies, H., and Jones, D.P. (2020). Reactive oxygen species (ROS) as pleiotropic physiological signalling agents. Nat. Rev. Mol. Cell Biol. *21*, 363–383.

Singh, J. (2021). Harnessing the power of genetics: fast forward genetics in Caenorhabditis elegans. Mol. Genet. Genomics *296*, 1–20.

Singh, J., and Aballay, A. (2017). Endoplasmic reticulum stress caused by lipoprotein accumulation suppresses immunity against bacterial pathogens and contributes to immunosenescence. MBio *8*, e00778-17.

Singh, J., and Aballay, A. (2019a). Microbial colonization activates an immune fight-and-flight response via neuroendocrine signaling. Dev. Cell *49*, 89–99.

Singh, J., and Aballay, A. (2019b). Intestinal infection regulates behavior and learning via neuroendocrine signaling. Elife *8*, e50033.

Trachootham, D., Lu, W., Ogasawara, M.A., Valle, N.R. Del, and Huang, P. (2008). Redox regulation of cell survival. Antioxidants Redox Signal. *10*, 1343–1374.

Ulrich, K., and Jakob, U. (2019). The role of thiols in antioxidant systems. Free Radic. Biol. Med. *140*, 14–27.

Villanueva, C., and Kross, R.D. (2012). Antioxidant-induced stress. Int. J. Mol. Sci. *13*, 2091–2109.

Wang, B., Pandey, T., Long, Y., Delgado-Rodriguez, S.E., Daugherty, M.D., and Ma, D.K. (2022). Co-opted genes of algal origin protect C. elegans against cyanogenic toxins. Curr. Biol. *32*, 4941-4948.e3.

Watson, E., Macneil, L.T., Ritter, A.D., Yilmaz, L.S., Rosebrock, A.P., Caudy, A.A., and Walhout, A.J.M. (2014). Interspecies systems biology uncovers metabolites affecting C. elegans gene expression and life history traits. Cell *156*, 759–770.

Winter, A.D., Tjahjono, E., Beltrán, L.J., Johnstone, I.L., Bulleid, N.J., and Page, A.P. (2022). Dietary-derived vitamin B12 protects Caenorhabditis elegans from thiol-reducing agents. BMC Biol. *20*, 228.

Yong, R., and Searcy, D.G. (2001). Sulfide oxidation coupled to ATP synthesis in chicken liver mitochondria. Comp. Biochem. Physiol. Part B Biochem. Mol. Biol. *129*, 129–137.

Zito, E. (2015). ERO1: A protein disulfide oxidase and H2O2 producer. Free Radic. Biol. Med. *83*, 299–304.

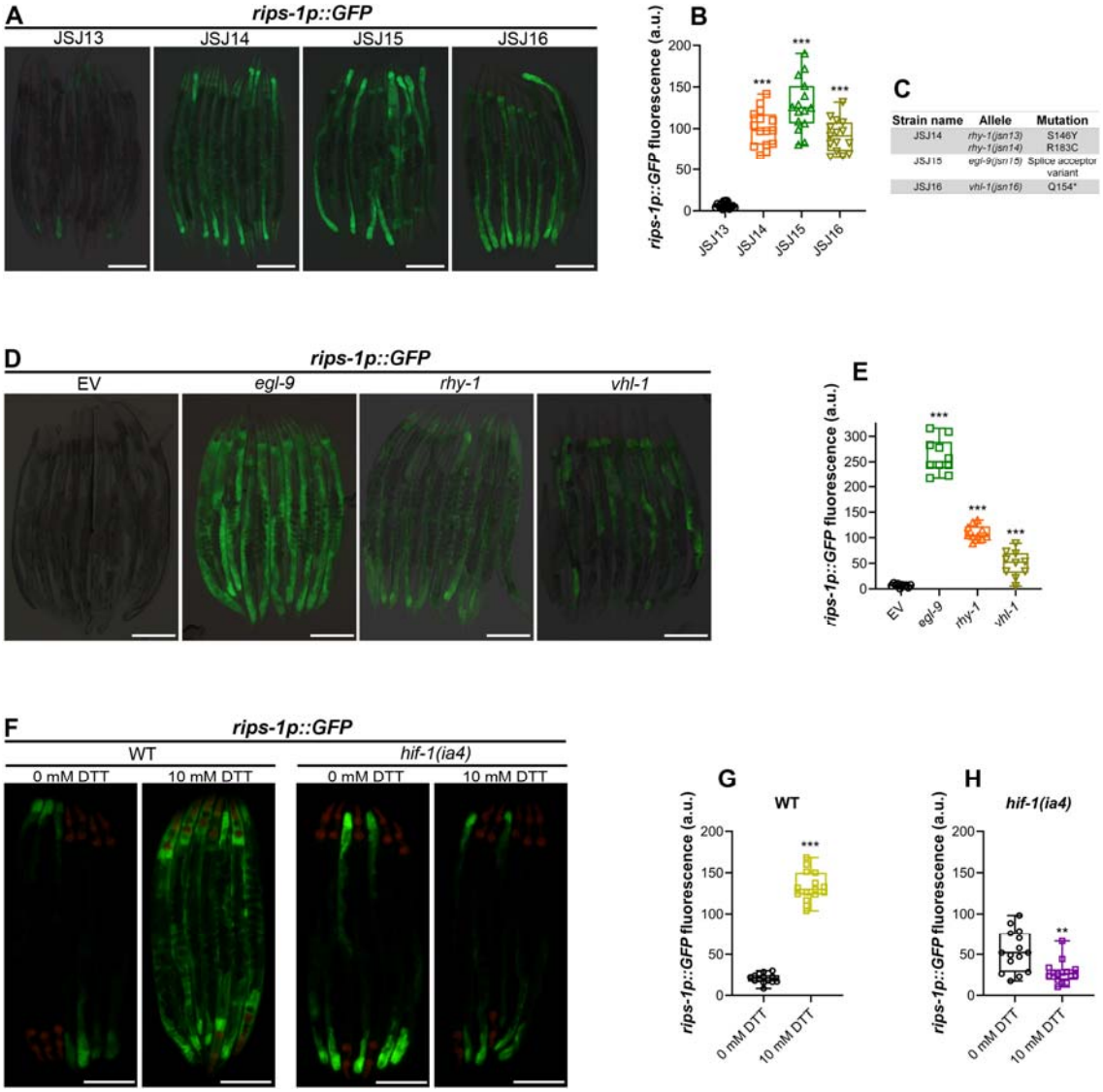

Figure 1. The hypoxia response pathway modulates *rips-1* expression levels

(A) Representative fluorescence images of the parental strain JSJ13 (*rips-1p::GFP*) and the mutants isolated from the forward genetic screen. The isolated mutants were designated JSJ14 to JSJ16. Scale bar = 200 µm.

(B) Quantification of GFP levels of *rips-1p::GFP* in JSJ13-JSJ16 animals. ***$p < 0.001$ via the *t*-test ($n = 15$ worms each).

(C) Table summarizing the alleles identified by whole-genome sequencing in JSJ14-JSJ16 strains.

(D) Representative fluorescence images of *rips-1p::GFP* animals following RNAi against *egl-9*, *rhy-1*, and *vhl-1*. Animals grown on empty RNAi vector (EV) were used as the control. Scale bar = 200 µm.

(E) Quantification of GFP levels of *rips-1p::GFP* animals following RNAi against *egl-9*, *rhy-1*, and *vhl-1*, along with EV control. ***$p < 0.001$ via the *t*-test ($n = 10$ worms each).

(F) Representative fluorescence images of *rips-1p::GFP* and *hif-1(ia4);rips-1p::GFP* animals grown on 0 mM DTT until the young adult stage, followed by incubation on 0 mM or 10 mM DTT for 10 hours. Scale bar = 200 μm.

(G) Quantification of GFP levels of *rips-1p::GFP* animals grown on 0 mM DTT until the young adult stage, followed by incubation on 0 mM or 10 mM DTT for 10 hours. ***$p < 0.001$ via the *t*-test ($n = 14$ worms for 0 mM DTT and 15 worms for 10 mM DTT).

(H) Quantification of GFP levels of *hif-1(ia4);rips-1p::GFP* animals grown on 0 mM DTT until the young adult stage, followed by incubation on 0 mM or 10 mM DTT for 10 hours. **$p < 0.01$ via the *t*-test ($n = 15$ worms each).

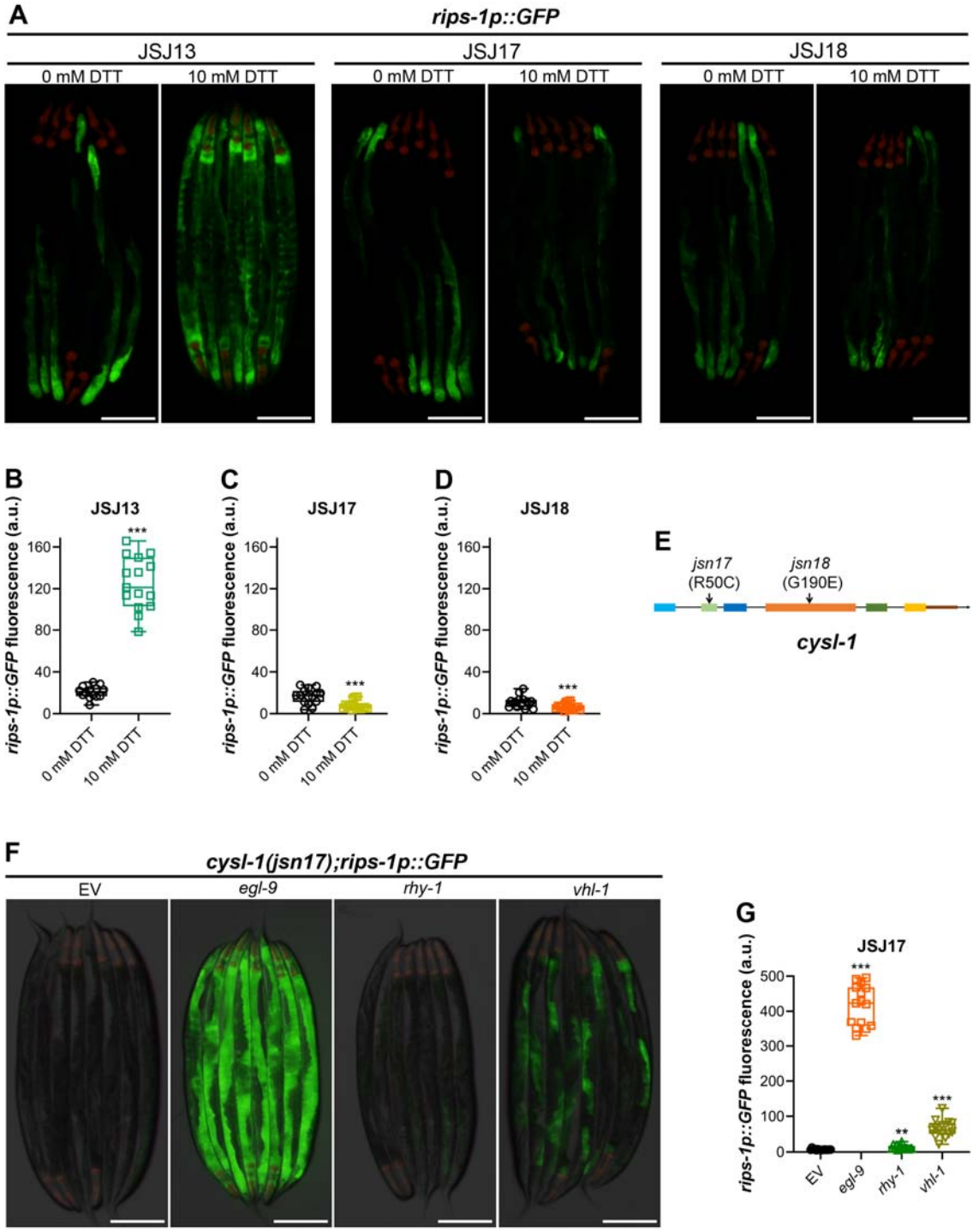

Figure 2. CYSL-1 is required for DTT-mediated *rips-1* upregulation

(A) Representative fluorescence images of the parental strain JSJ13 (*rips-1p::GFP*) and the isolated mutants, JSJ17 and JSJ18, grown on 0 mM DTT until the young adult stage, followed by incubation on 0 mM or 10 mM DTT for 10 hours. Scale bar = 200 µm.

(B-D) Quantification of GFP levels of *rips-1p::GFP* in JSJ13 (B), JSJ17 (C), and JSJ18 (D) animals grown on 0 mM DTT until the young adult stage, followed by incubation on 0 mM or 10 mM DTT for 10 hours. ***$p < 0.001$ via the *t*-test (n = 14-15 worms each).

(E) Mapping of the *cysl-1* alleles identified in the forward genetic screen.

(F) Representative fluorescence images of JSJ17 (*cysl-1(jsn17);rips-1p::GFP*) animals following RNAi against *egl-9*, *rhy-1*, and *vhl-1*, along with EV control. Scale bar = 200 µm.

(G) Quantification of GFP levels of JSJ17 (*cysl-1(jsn17);rips-1p::GFP*) animals following RNAi against *egl-9*, *rhy-1*, and *vhl-1*, along with EV control. ***$p < 0.001$ and **$p < 0.01$ via the *t*-test (n = 15 worms each).

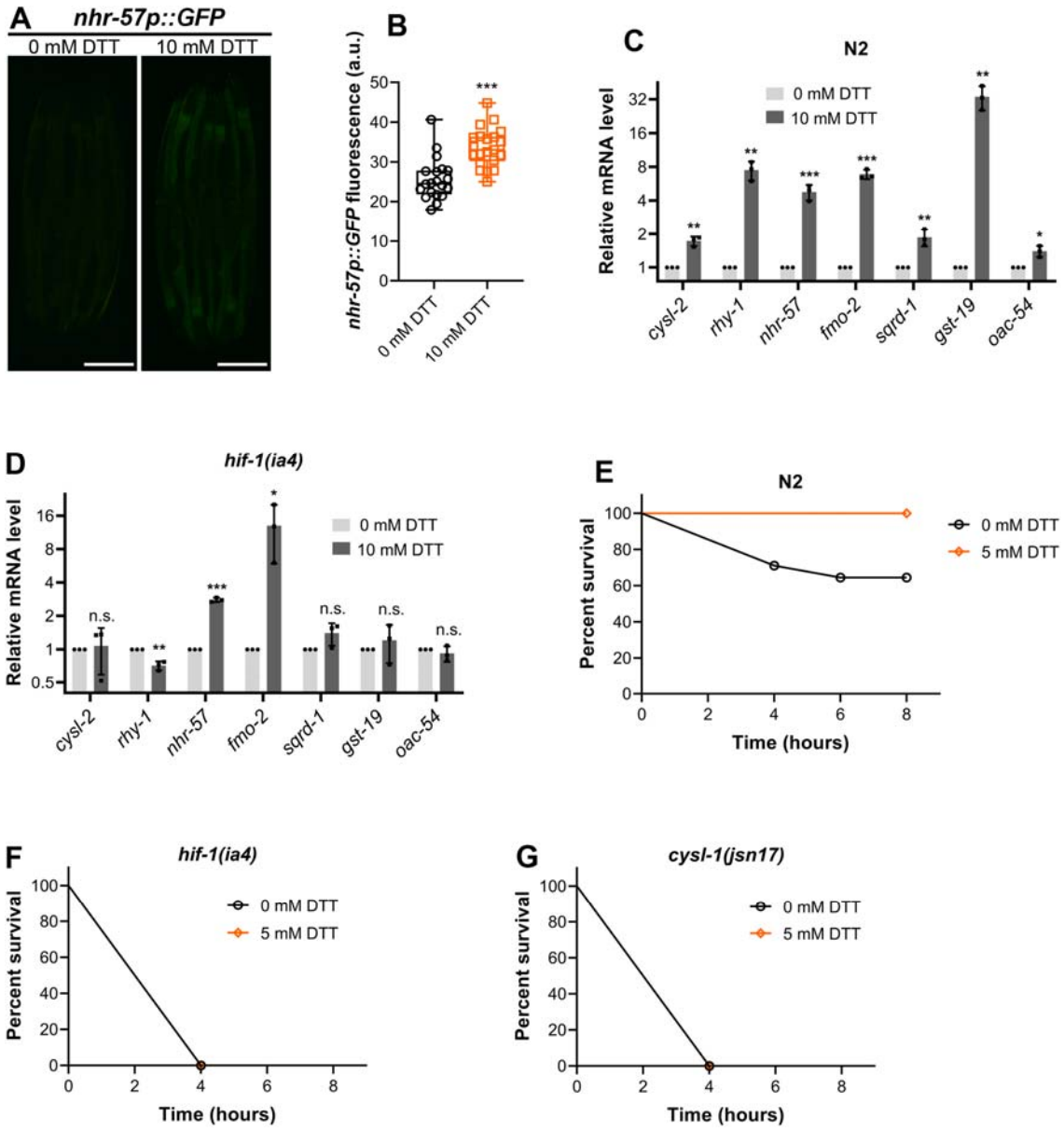

Figure 3. Thiol reductive stress activates the hypoxia response pathway

(A) Representative fluorescence images of *nhr-57p::GFP* animals grown on 0 mM DTT until the young adult stage, followed by incubation on 0 mM or 10 mM DTT for 12 hours. Scale bar = 200 µm.

(B) Representative fluorescence images of *nhr-57p::GFP* animals grown on 0 mM DTT until the young adult stage, followed by incubation on 0 mM or 10 mM DTT for 12 hours. ***$p < 0.001$ via the *t*-test ($n = 20$ worms for 0 mM DTT and 21 worms for 10 mM DTT).

(C-D) Gene expression analysis of N2 (C) and *hif-1(ia4)* (D) animals grown on 0 mM DTT until the young adult stage, followed by incubation on 0 mM or 10 mM DTT for 10 hours. ***$p < 0.001$, **$p < 0.01$, and *$p < 0.05$ via the *t*-test. n.s., nonsignificant ($n = 3$ biological replicates).

(E-G) Representative survival plots of N2 (E), *hif-1(ia4)* (F), and *cysl-1(jsn17)* (G) animals on *P. aeruginosa* PAO1 under fast-killing assay conditions. Prior to transfer to *P. aeruginosa* PAO1 lawns at the L4 stage, the animals were grown on *Comamonas aquatica* DA1877 diet containing 0 mM or 5 mM DTT. The plots of *hif-1(ia4)* and *cysl-1(jsn17)* animals are identical, as all the animals (from 0 mM and 5 mM DTT) are dead by the first time point (4 hours) for both the mutants.

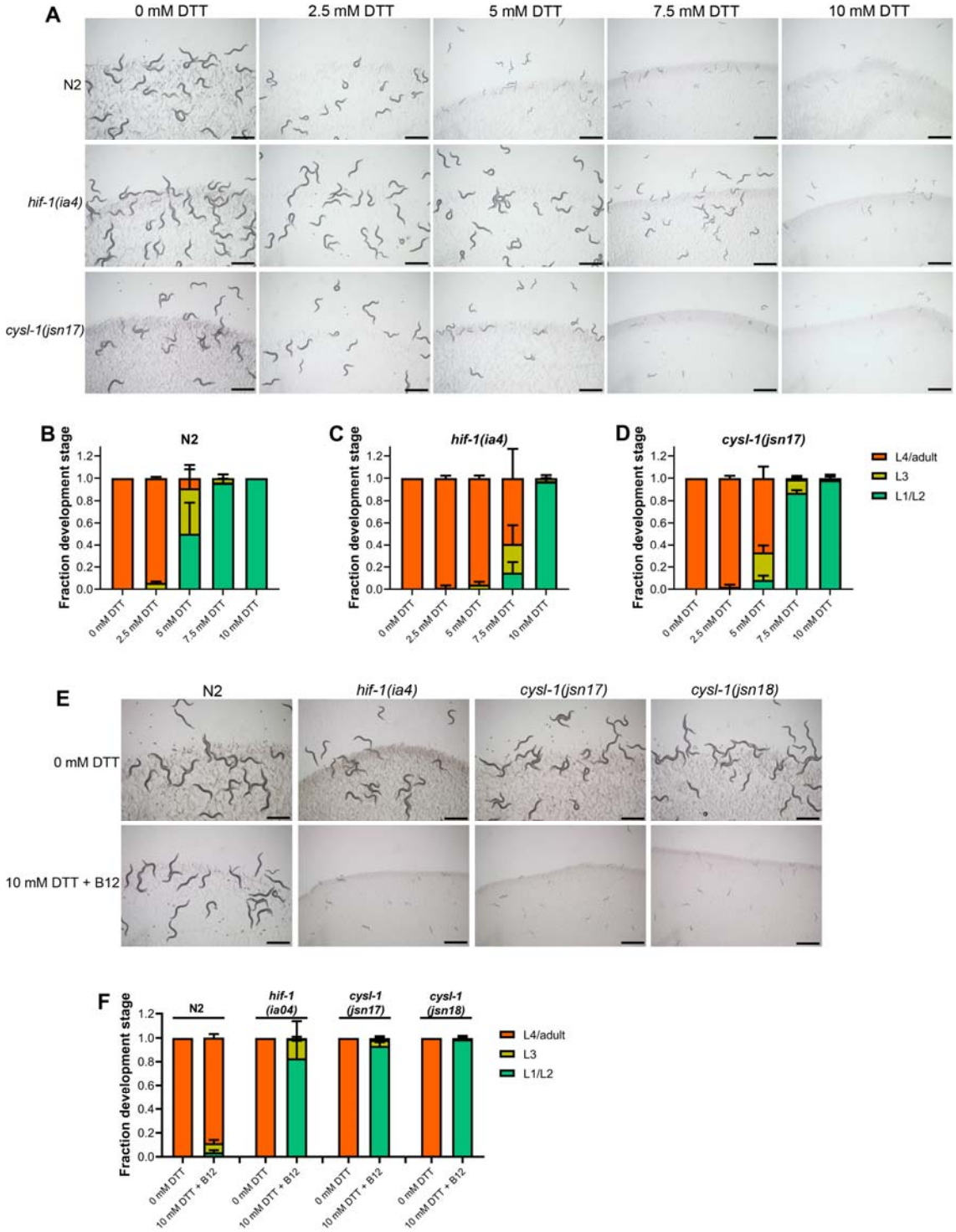

Figure 4. Hypoxia response pathway protects against thiol reductive stress

(A) Representative images of N2, *hif-1(ia4)*, and *cysl-1(jsn17)* animals on various concentrations of DTT on *E. coli* OP50 diet after 72 hours of hatching at 20°C. Scale bar = 1 mm.

(B-D) Quantification of different developmental stages of N2 (B), *hif-1(ia4)* (C), and *cysl-1(jsn17)* (D) animals on various concentrations of DTT on *E. coli* OP50 diet after 72 hours of hatching at 20°C. (*n* = 3 biological replicates; animals per condition per replicate >100).

(E) Representative images of N2, *hif-1(ia4)*, *cysl-1(jsn17)*, and *cysl-1(jsn18)* animals after 72 hours of hatching at 20°C on *E. coli* OP50 diet containing 0 mM DTT and 10 mM DTT supplemented with 50 nM vitamin B12. Scale bar = 1 mm.

(F) Quantification of different developmental stages of N2, *hif-1(ia4)*, *cysl-1(jsn17)*, and *cysl-1(jsn18)* animals after 72 hours of hatching at 20°C on *E. coli* OP50 diet containing 0 mM DTT and 10 mM DTT supplemented with 50 nM vitamin B12. (*n* = 3 biological replicates; animals per condition per replicate >100).

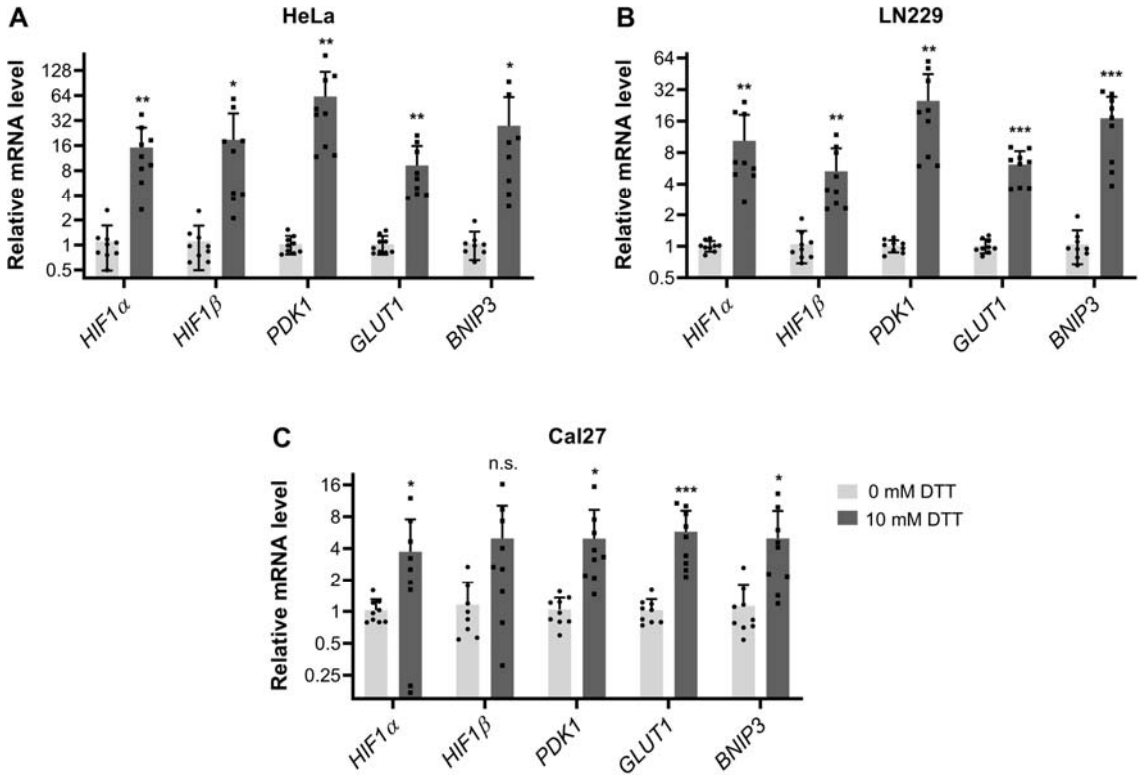

Figure 5. Thiol reductive stress activates the hypoxia response pathway in human cell lines

(A-C) Gene expression analysis of HeLa (A), LN229 (B), and Cal27 (C) cell lines with and without exposure to 10 mM DTT for 24 hours. ***$p < 0.001$, **$p < 0.01$, and *$p < 0.05$ via the *t*-test. n.s., nonsignificant ($n = 3$ biological replicates with 2-3 technical repeats each).

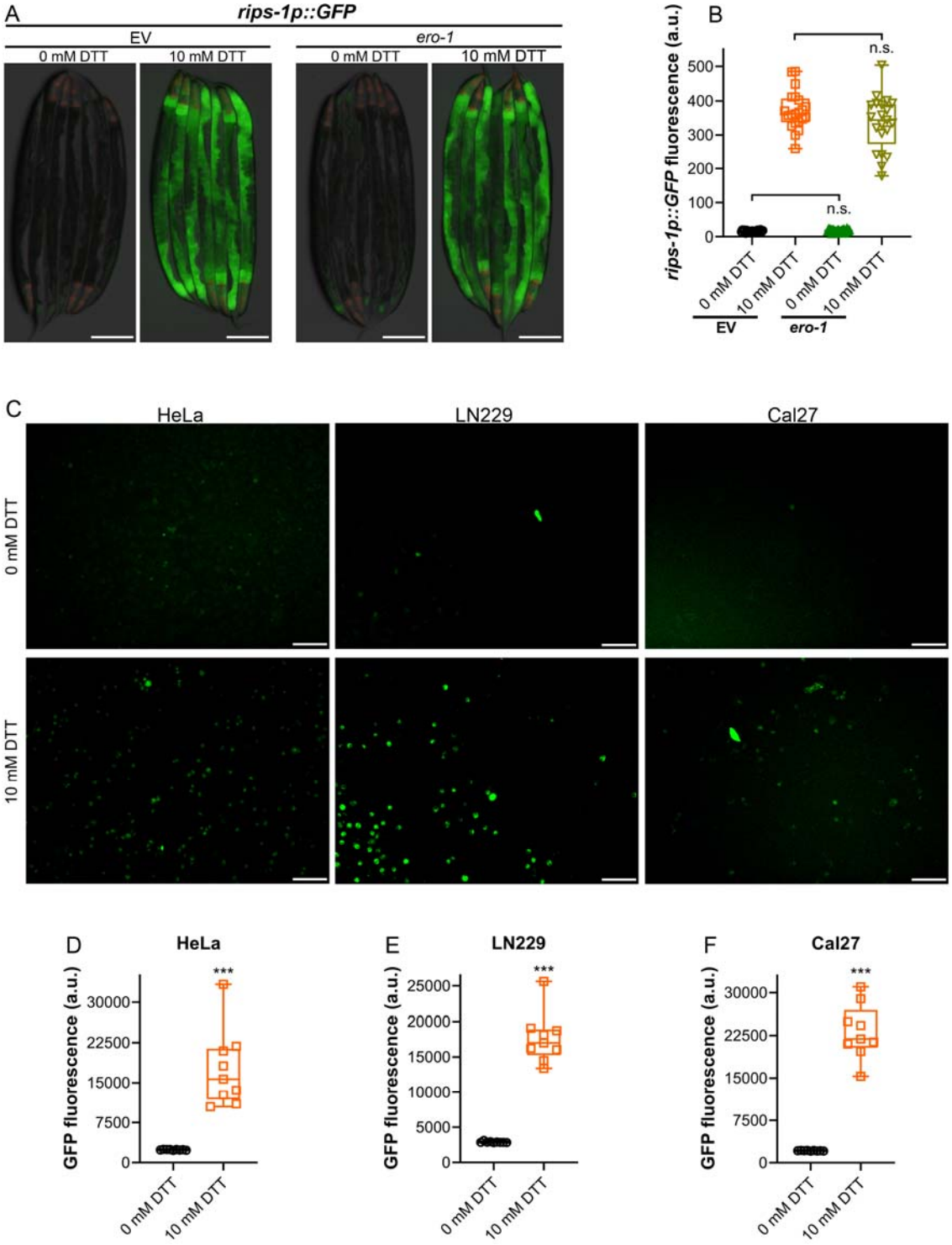

Figure 6. Thiol reductive stress depletes cellular oxygen

(A) Representative fluorescence images of *rips-1p::GFP* animals grown on EV and *ero-1* RNAi plates containing 0 mM DTT until the young adult stage, followed by incubation

on the corresponding RNAi plates containing 0 mM or 10 mM DTT for 12 hours. Scale bar = 200 µm.

(B) Quantification of GFP levels of *rips-1p::GFP* animals grown on EV and *ero-1* RNAi plates containing 0 mM DTT until the young adult stage, followed by incubation on the corresponding RNAi plates containing 0 mM or 10 mM DTT for 12 hours. n.s., nonsignificant via the *t*-test (n = 21 worms each).

(C) Representative fluorescence images of HeLa, LN229, and Cal27 cell lines upon treatment with image-iT™ green hypoxia reagent. The cells were pretreated with 0 mM or 10 mM DTT for 24 hours prior to fixation with image-iT™ green hypoxia reagent. Scale bar = 100 µm.

(D-F) Quantification of GFP levels of image-iT™ green hypoxia reagent-treated HeLa (D), LN229 (E), and Cal27 (F) cell lines. The cells were pretreated with 0 mM or 10 mM DTT for 24 hours prior to fixation with image-iT™ green hypoxia reagent. ***$p < 0.001$ via the *t*-test (n = 9 wells each).

Supplementary Figures:

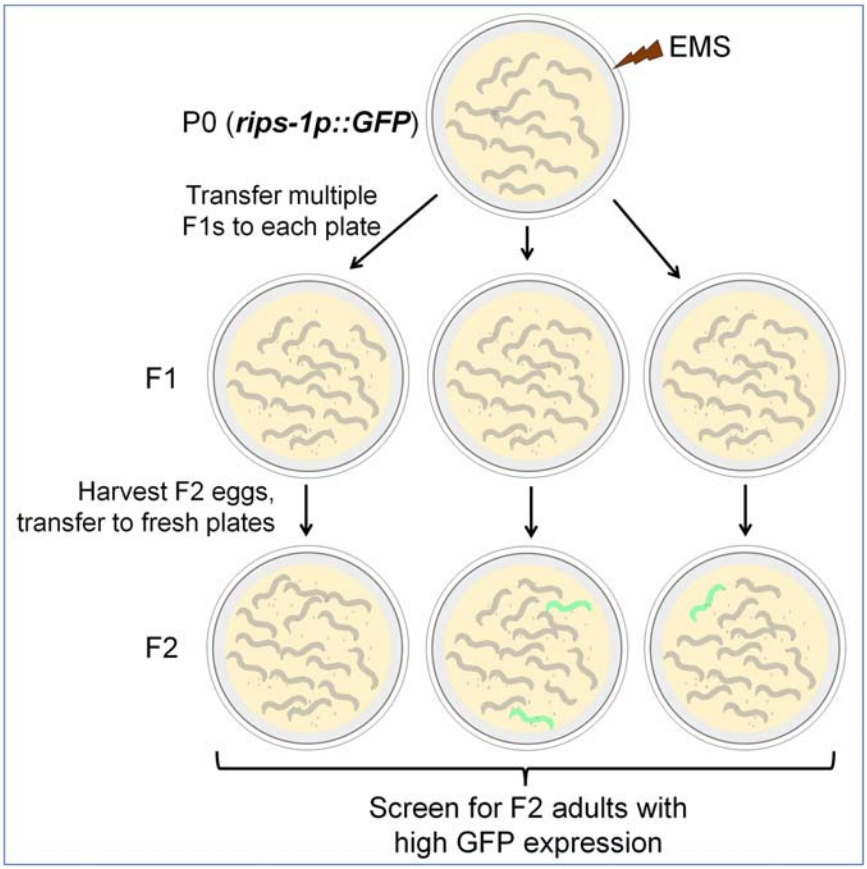

Figure S1. Scheme for a forward genetic screen for mutants with constitutive upregulation of *rips-1p::GFP*

The genetic screen is designed to isolate high GFP animals in the F2 generation of EMS-mutagenized *rips-1p::GFP* worms.

.

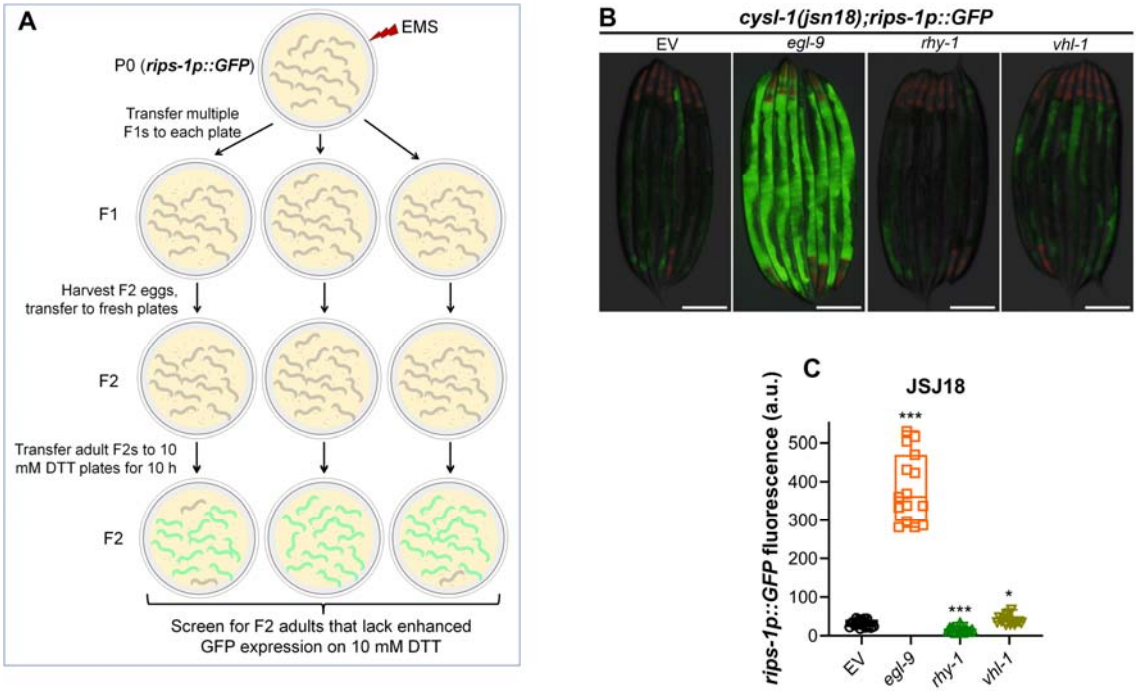

Figure S2. CYSL-1 is required for DTT-mediated *rips-1* upregulation

(A) Scheme for a forward genetic screen for mutants that lack upregulation of *rips-1p::GFP* on 10 mM DTT.

(B) Representative fluorescence images of JSJ18 (*cysl-1(jsn18);rips-1p::GFP*) animals following RNAi against *egl-9*, *rhy-1*, and *vhl-1*, along with EV control. Scale bar = 200 µm.

(C) Quantification of GFP levels of JSJ18 (*cysl-1(jsn18);rips-1p::GFP*) animals following RNAi against *egl-9*, *rhy-1*, and *vhl-1*, along with EV control. ***$p < 0.001$ and *$p < 0.05$ via the *t*-test ($n = 15$ worms each).

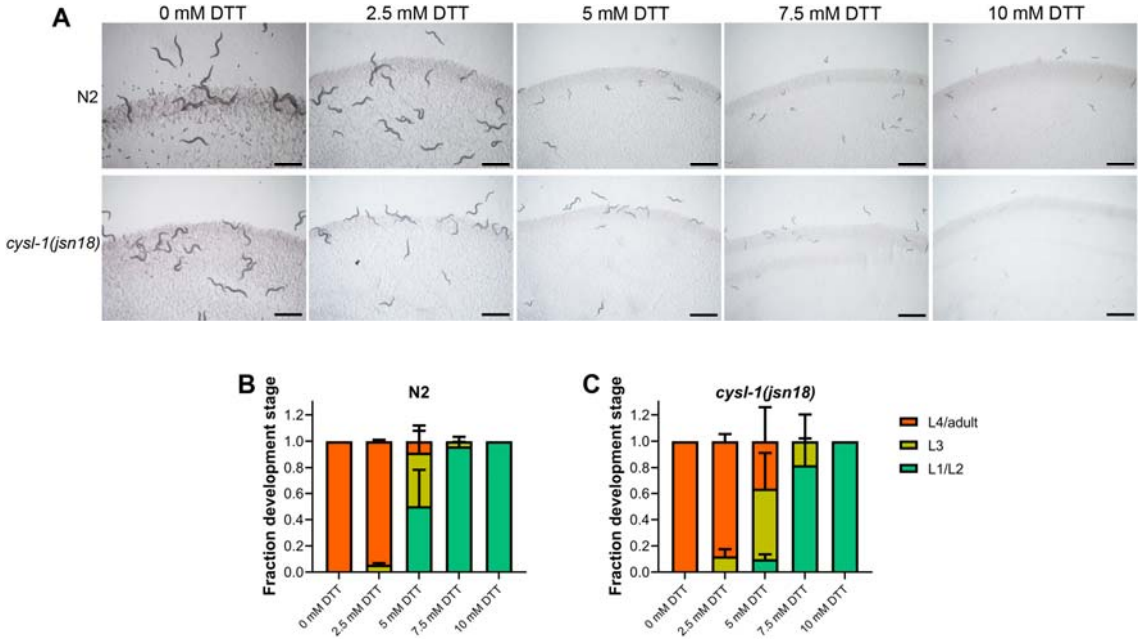

Figure S3. *cysl-1(jsn18)* animals develop better than N2 animals at 5 mM DTT

(A) Representative images of N2 and *cysl-1(jsn18)* animals on various concentrations of DTT on *E. coli* OP50 diet after 72 hours of hatching at 20°C. Scale bar = 1 mm.

(B-C) Quantification of different developmental stages of N2 (B) and *cysl-1(jsn18)* (C) animals on various concentrations of DTT on *E. coli* OP50 diet after 72 hours of hatching at 20°C. The N2 data in (B) are the same as in Figure 4B. (n = 3 biological replicates; animals per condition per replicate >100).

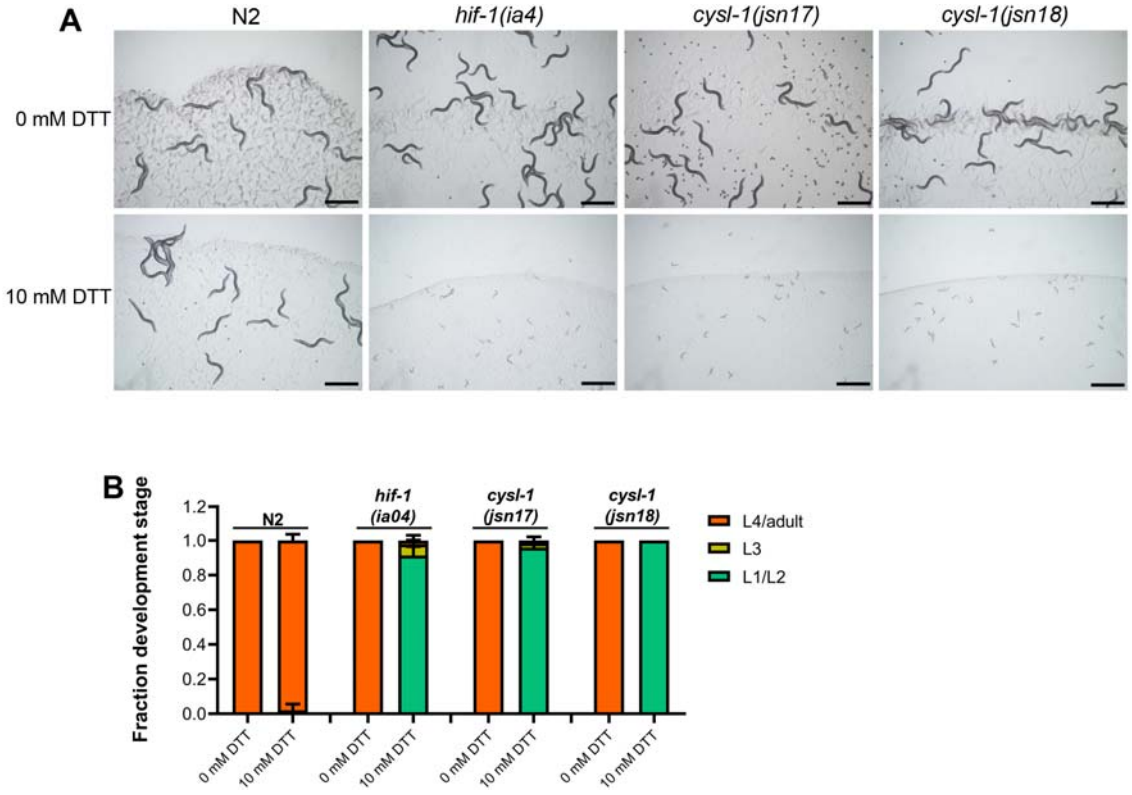

Figure S4. Hypoxia response pathway protects against thiol reductive stress

(A) Representative images of N2, *hif-1(ia4)*, *cysl-1(jsn17)*, and *cysl-1(jsn18)* animals after 72 hours of hatching at 20°C on *C. aquatica* DA1877 diet containing 0 mM or 10 mM DTT. Scale bar = 1 mm.

(B) Quantification of different developmental stages of N2, *hif-1(ia4)*, *cysl-1(jsn17)*, and *cysl-1(jsn18)* animals after 72 hours of hatching at 20°C on *C. aquatica* DA1877 diet containing 0 mM or 10 mM DTT. (n = 3 biological replicates; animals per condition per replicate >100).

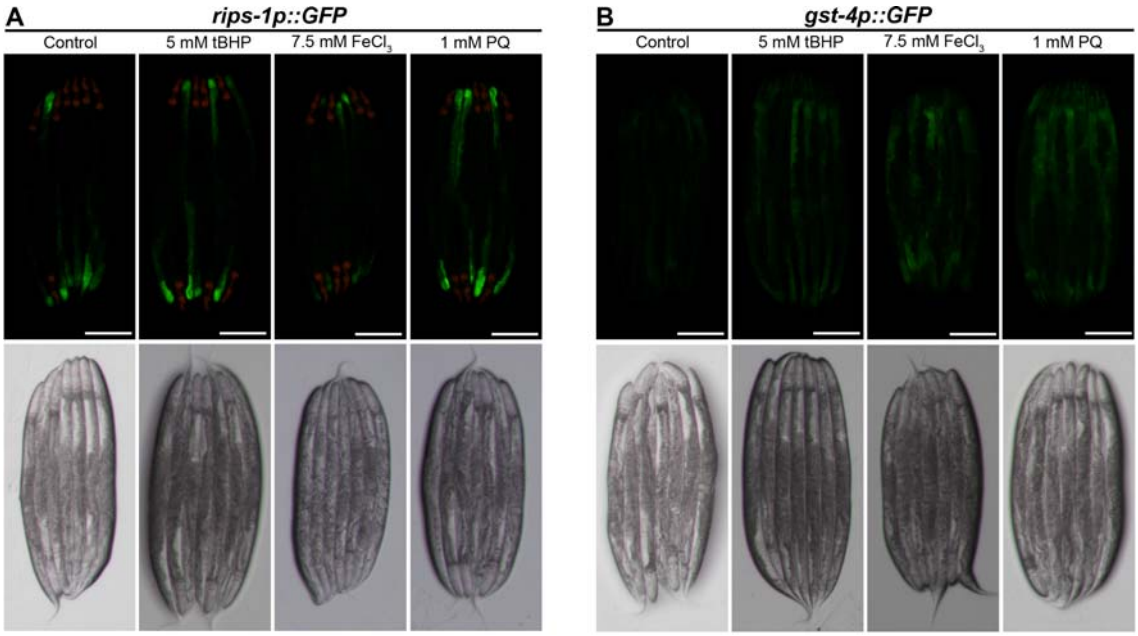

Figure S5. Oxidative stress does not regulate *rips-1p::GFP* expression

(A) Representative fluorescence (top) and the corresponding brightfield (bottom) images of *rips-1p::GFP* animals grown on *E. coli* OP50 diet without any supplements until the young adult stage, followed by incubation on *E. coli* OP50 diet containing no supplement (control), 5 mM tert-butyl hydroperoxide (tBHP), 7.5 mM ferric chloride ($FeCl_3$), or 1 mM paraquat (PQ) for 12 hours. Scale bar = 200 µm.

(B) Representative fluorescence (top) and the corresponding brightfield (bottom) images of *gst-4p::GFP* animals grown on *E. coli* OP50 diet without any supplements until the young adult stage, followed by incubation on *E. coli* OP50 diet containing no supplement (control), 5 mM tBHP, 7.5 mM $FeCl_3$, or 1 mM PQ for 12 hours. Scale bar = 200 µm.

Table S1: Primers used in the study

Primer for quantitative reverse transcription-PCR in *C. elegans*		
Gene name	Forward primer sequence (5'-3')	Reverse primer sequence (5’-3’)
Pan-act	TCGGTATGGGACAGAAGGAC	CATCCCAGTTGGTGACGATA
cysl-2	GATGCCAGCGTCGATGAGTA	AGCTCTTCGGCTCTTTGGAC
rhy-1	TGGAACGACTCAGCGAAGTG	GACGACAAGTGTCATCCATGC
nhr-57	GCGATGAAAATGTACCGCCC	TCCGGCTGACCATCTAGTGA
fmo-2	TCCAGTTCTTGGTCTTCGCC	AGGCTCCGGTTTGGTTGTAG
sqrd-1	GGTGGAGGCTGTTTGTGTGTA	ACCGGGTAAACAAGACGCAG
gst-19	CGCGGATCTTGTAGTCGTCA	ATTCCTTGATCCCTGGCTGC
oac-54	TCTATGTTCATCCGTGCGGG	AACTGCGGGATCTTGTCCTG
Primer for quantitative reverse transcription-PCR in human cell lines		
Gene name	Forward primer sequence (5'-3')	Reverse primer sequence (5’-3')
Beta-actin	CAAGAGATGGCCACGGCTGCT	TCCTTCTGCATCCTGTCGGCA
HIF1α	TATGAGCCAGAAGAACTTTTAGGC	CACCTCTTTTGGCAAGCATCCTG
HIF1β	CTGTCATCCTGAAGACCAGCAG	CTGGTTCTCATCCAGAGCCATTC
PDK1	CATGTCACGCTGGGTAATGAGG	CTCAACACGAGGTCTTGGTGCA
GLUT1	TTGCAGGCTTCTCCAACTGGAC	CAGAACCAGGAGCACAGTGAAG
BNIP3	TCAGCATGAGGAACACGAGCGT	GAGGTTGTCAGACGCCTTCCAA